——Note——

Aerodynamical Coefficients of A Circular Cylinder with Tangential Injection

by

Fumio YOSHINO and Ryoji WAKA

(Recived October 31 1972)

Summary

There is presented the half of the investigation that had been carried out on the flow around and the aerodynamic force acting on a circular cylinder with tangential injection of air. The coefficients of the aerodynamic forces were found to peculiarly behave according to the position of the slot especially when the intensity of the injection is weak.

1 Introduction

It has been well known that when the jet is injected to the tangential direction on the circular cylinder, it flows along the cylinder. This is the so-called Coanda effect. Making use of it, we can control the boundary layer and get the high lift on a circular cylinder. Dunham[1] and others carried out the investigation on this subject. It is also tried to increase the lift-drag ratio by the other researchers.[2]

However, we can scarcely find the detailed investigation that the position of the slot is extensively varied at small value of C_μ, especially in the flow with good two-dimensionality.

In this report, the experimental investigation has been systematically carried out on the flow around the circular cylinder and aerodynamic force acting on it when the intensity of jet and the position of slot are varied at rather small Reynolds number, while two-dimensionality of the flow being carefully kept.

2 Nomenclature

C_μ : Momentum coefficient of the jet $\left(= \dfrac{W_J{}^2 \rho_J S}{\frac{1}{2} \rho_a U_\infty^2 D} \right)$

C_L : Sectional lift coefficient $\left(= \frac{\text{(Lift)}}{\frac{1}{2}\rho_a U_\infty^2 Db} \right)$

C_D : Drag coefficient $\left(= \frac{\text{(Drag)}}{\frac{1}{2}\rho_a U_\infty^2 Db} \right)$

C_P : Static-pressure coefficient $\left(= \frac{\Delta P}{\frac{1}{2}\rho_a U_\infty^2} \right)$

C_{pb} : Static-pressure coefficient of the base pressure

ρ_a : Atmospheric density $\left(= \frac{P_a}{gR_C T} \right)$

ρ_J : Density of the jet $\left(= \rho_W \left(\frac{P_a}{P_W} \right)^{\frac{\kappa-1}{\kappa}} \right)$

ρ_W : Density of the compressed air inside circular cylinder

ν : Coefficient of kinematic viscosity

σ : Specific gravity of alcohol

κ : Specific-heat ratio

Λ^* : Effective aspect ratio of the end plate

Λ : Aspect ratio of the end plate

U : Velocity of the wind tunnel

W_J : Velocity of the jet

P_a : Atmospheric pressure

P_W : Pressure inside the circular cylinder

T : Absolute temperature in the wind tunnel

T_W : Absolute temperature of the compressed air

θ_J : Position of the slot (see Fig. 1)

θ, θ_{sep}, θ_{st} : Angle measured from the vertical plane passing through the axis of the circular cylinder, the angles of the separation point and the stagnation point respectively (downstream is plus)

D : Diameter of the circular cylinder

R, b : Radius and span of the circular cylinder

S : Width of the slot

l : Length of the end plate

h : Height of the end plate

Z : Distance from the center of the span in the spanwise direction (starboard is plus)

y : Distance of the wall in the radial direction

R_c : Gas constant of air

R_e : Reynolds number $\left(= \frac{U_\infty D}{\nu} \right)$

3 Experimental

Fig. 1 shows the section of the model cylinder. The small cylinder, 25mm in diameter, is tangentially in contact with the inside of the large pipe, 100mm in diameter and this small cylinder makes a part of the nozzle wall.

The jet is injected from the slot along the large cylinder. The slot has a constant width, 0.55mm wide, over the whole span.

The outside of model cylinder is made like a mirror surface by chrome-plating.

The cylinder is 404mm long in the spanwise direction and has 35 static-pressure holes on the circumference at the center of the span.

The end plates with aerofoil section are installed at both ends of the cylinder (see Fig. 2). Those dimensions are 62mm thick, 726mm long and 362mm high.

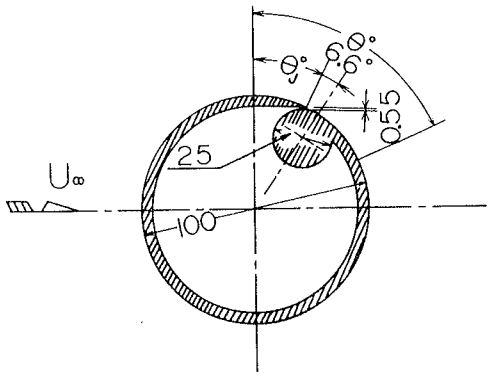

Fig. 1 Cross-sectin of the circular cylinder.

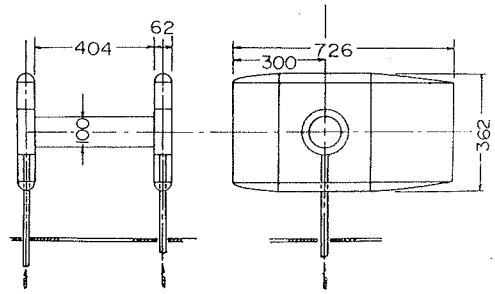

Fig. 2 Circular cylinder with end plates.

The struts are connected with the cylinder in the inside of the end plates and are fixed on the three-components balance after passing through the bottom of the end plates and the floor of the wind tunnel.

The inside of the strut is hollow through which the compressed air is supplied with into the cylinder. The test section of the wind tunnel has the dimension of 1.0×0.7m in the cross-section and is 1.5m long. The maximum tunnel speed is measured about 52m/s.[3]

The measurements of the aerodynamic force and the velocity distribution were made with the three-components balance and the total-pressure pitot tube respectively.

The experiments were carried out under the comparatively low R_e that is 3.2×10^5, since it was found from our preliminary experiments and Tanner's one[4] that if the boundary layer were turbulent, it was difficult to keep the two-dimensionality of the flow.

To observe the influence of R_e, the measurements were made at the other R_e'

s, too, that is, 2.6×10^5 and 1.9×10^5.

The measurements of the aerodynamic force were made at the six positions of the slot, that is, $\theta_J = -40°$, $-20°$, $0°$, $10°$, $20°$ and $30°$ by properly varying C_μ from 0 through about 0.46.

The static-pressure distribution in the flow direction (the circumferencial direction) were measured in each case.

To determine the aerodynamic force acting on the cylinder alone, we made two kinds of measurements as follows.

First, the tare, that is, the aerodynamic force acting on the strut and end plates etc. were measured without the cylinder.

Secondly, the aerodynamic force acting on the cylinder together with the strut and the end plates etc. were measured. Then, the aerodynamic force on the cylinder alone was obtained by subtracting the former values from the latter ones.

Therefore, we can not avoid a little error in the drag. To be sure, the lift and drag were calculated from the static-pressure distribution, too.

4 Results and Discussion

Fig. 3 shows the values of C_L and C_D which were measured by the balance whereas Fig. 4 shows the values calculated from the static-pressure distribution. Both

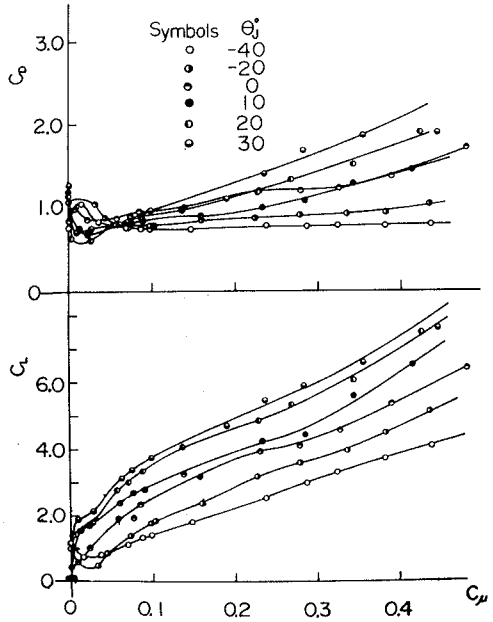

Fig. 3 Lift (below) and drag(above) coefficients by the balance.

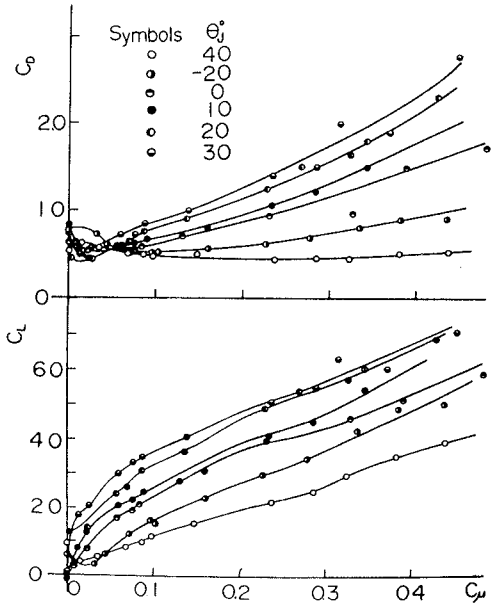

Fig. 4 Lift (below) and drag (above) coefficients due to static pressure.

values of C_L agree with each other, while the tendencies of both C_D's resemble but their values are different from each other, the reasons of which are thought as follows.

First, it is evident that the flow over the cylinder surface is nearly two dimensional from the measurement of the velocity distribution (to be published) that was made at the same time as the measurement of the aerodynamic force.

Second, we have the following empirical formula on the effective aspect ratio due to the end plates,

$$\Lambda^* = \Lambda \left[1 + \frac{1}{2}\frac{h}{l}\left(\frac{l}{D}\right)^2\right] \tag{1}$$

, which gives $\Lambda^* \fallingdotseq 57$ in our model, so that it is also known that the flow around the cylinder is nearly two-dimensional.

Therefore, something other than the three-dimensionality of the flow is to be the main reason of the discrepancy between the values of C_L and C_D measured by the balance and calculated from the static-pressure distribution. In this model used for the experiment, the aerodynamic force acting on the cylinder must be the resultant one of the force due to the static pressure on the cylinder surface and the thrust due to the reaction of the jet at the outlet of the slot.

Therefore, C_L and C_D are expressed as follows.

$$C_L = C_{LS} - C_{LJ} \tag{2}$$

$$C_D = C_{DS} - C_{DJ} \tag{3}$$

where $C_{JL} = C_\mu \sin\alpha$, $C_{DJ} = C_\mu \cos\alpha$, $\alpha = 23.37° - \theta_J$ and C_{LS} and C_{DS} are the lift and drag coefficients due to the static pressure on the cylinder respectviely, C_{LS} and C_{DS} are the lift and drag coefficients calculated from the static-pressure distribution and C_L and C_D are the lift and drag coefficients by the balance.

In the above equations, it is found that C_{LJ} and C_{DJ} are proportional to C_μ, if θ_J is fixed.

Therefore the values measured by the balance and calculated from the static-pressure distribution are nearly equal to each other.

On the other hand, the proportion of C_{DS} in C_D is large and it is clear from the equation (3) that C_{DJ} is small in case of the small θ_J but is large when θ_J is large. And C_{DJ} becomes large proportionally to C_μ.

Hence, the larger the θ_J is and the larger the C_μ is, the smaller the value of C_D measured by the balance is in comparison with the value of C_D calculated from the static-pressure distribution (see Fig. 3.).

The qualitative analysis as mentioned above does not explain the difference between the values measured by the balance and those calculated from the static-pressure distribution in case of $C_\mu = 0$, for exsample see Figs. 3 and 4. This difference seems due to the method to have determined the aerodynamic force acting on the cylinder and the experimental error, which must especially make the error of C_D

large.

From the fact mentioned above, the values of C_{LJ} and C_{DJ} added to the values of C_{LS} and C_{DS} calculated from the static-pressure distribution seems nearer the true values than those measured by the balance.

4-1 On the lift coefficient, C_L

It is seen from Fig. 4 that C_L on the cylinder peculiarly behaves at small C_μ depending on each θ_J.

In case of $\theta_J \leqq -20°$, as C_μ increases starting from 0 (at $C_\mu = 0$, there is no injection of jet) C_L decreases once, reaches the minimum value and increases again.

On the other hand, in case of $\theta_J \geqq 0°$, as C_μ increases a little from 0, C_L increases rapidly and increases by degrees after C_μ reaches about 0.06, which results in the high lift by a little injection of air.

To make the following analysis easy, the section is divided into two subsections, that is, (1) The case of $\theta_J \leqq -20°$ and (2) The case of $\theta_J \geqq 0°$.

(1) The case of $\theta_J \leqq -20°$

It is known that the laminar and turbulent separations generally occur at $\theta \fallingdotseq -20° \sim 0°$ and $20° \sim 40°$ on the cylinder in the uniform flow respectively. This experiment is mainly carried out on $R_e = 3.2 \times 10^5$, so that the boudary layer is thought as laminar.

This is evident from the curve of $C_\mu = 0$ in Fig. 5c for $\theta_J \geqq 0°$.

However, when $\theta_J \leqq -20°$, the laminar flow passed the slot turns to the turbulent flow by the slot which plays the role of a tripwire.

There are many evidences of the turbulent boundary layer.

First, the negative pressure of the upper side having the slot is very large, which is seen from the curve of $C_\mu = 0$ in Fig. 5a.

Secondly, the separation point moves to downstream to about $25° \sim 30°$ in Fig. 8.

Thirdly, the base pressure is higher than that in the laminar separation (see Fig. 10).

On the other hand, the boundary layer is still laminar on the lower side of the cylinder (the side without the slot), so that the separation point of the lower side will be relatively more upstream than that of the upper side.

Thereby, the static-pressure distributions on the upper and lower sides of the cylinder are asymetric. For example, this is obvious from the curve of $C_\mu = 0$ when $\theta_J = -40°$ in Fig. 5a.

Therefore, the circulation is generated around the cylinder and the front-stagnation point, θ_{st}, will farther move to the negative side of θ than $-90°$. This is made sure in Fig.9, that is, when $C_\mu = 0$, the front-stagnation point moves to the negative side of θ by about $2.5° \sim 5°$ from $-90°$. Hence, the lift exists even in $C_\mu = 0$.

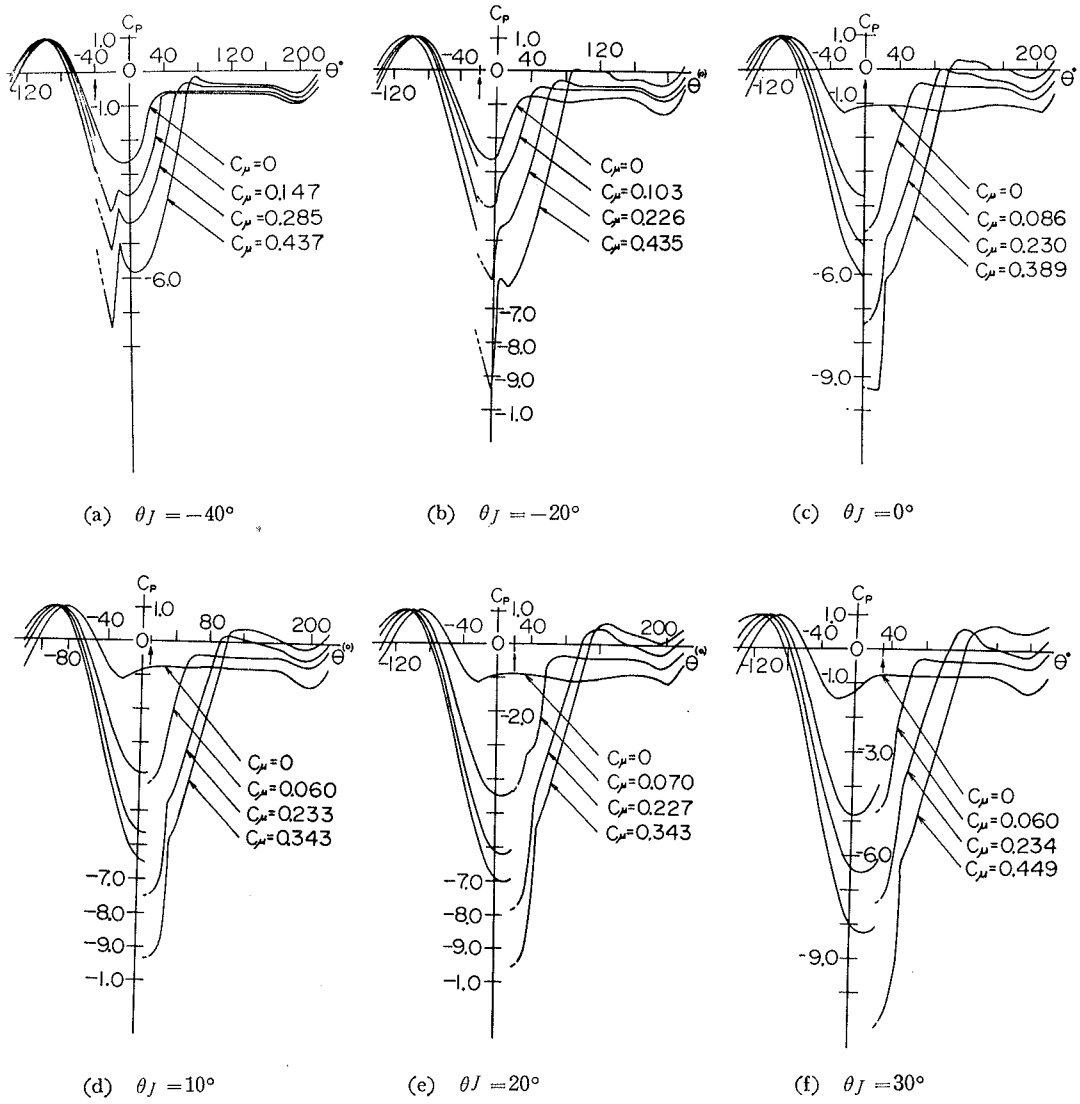

(a) $\theta_J = -40°$ (b) $\theta_J = -20°$ (c) $\theta_J = 0°$

(d) $\theta_J = 10°$ (e) $\theta_J = 20°$ (f) $\theta_J = 30°$

Fig. 5 Static-pressure distributions.

Next, when the air is injected but C_μ is very small, the velocity of the jet is lower than the velocity of the boundary layer of the main flow, hence, the jet can not increase the momentum of the boundary layer in the flow direction but decreases it, which therefore turns out to be the earlier separation than when $C_\mu = 0$.

It is obvious from the fact that the separation point moves to upstream as seen in Fig. 8. Fig. 10 indicates the similar result, too.

Fig. 6 shows the static-pressure distribution around the cylinder when $\theta_J = -40°$ and C_u is very small.

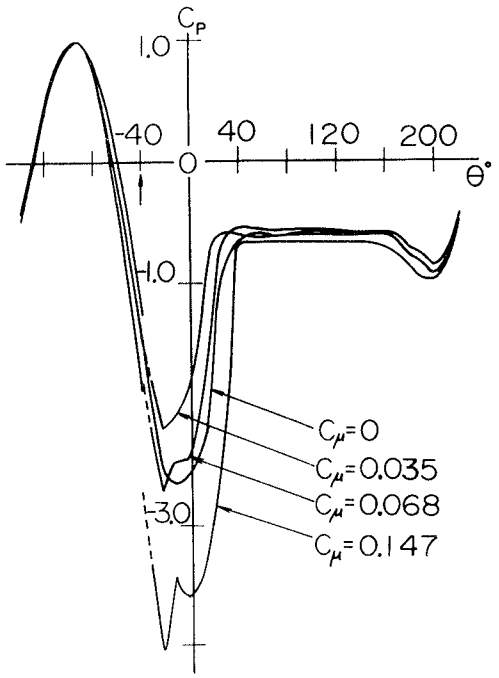

Fig. 6 Static-pressure distributions at small C_μ 's when $\theta_J = -40°$.

The curves of C_μ = 0.035 and 0.068 in the figure show, the negative pressure right after the slot is decreased from that of C_μ = 0 and that the separation point tends to move upstream.

Hence, as the circulation around the cylinder is decreased from that of C_μ = 0, the front-stagnation point is to approach the point of $\theta = -90°$. This is indicated in Fig. 9.

Therefore when C_μ is very little, the lift is seen to decreased by injecting air as in Fig. 4.

On the other hand, as C_μ increases further, it is evident that all C_L 's increase in the same way independently of θ_J (see Fig. 3 and Fig. 4).

This corresponds to the fact that the curves of θ_{sep} of each θ_J are mutually, nearly parallel when C_μ is large as in Fig. 8.

Table 1 indicates the intervals between the adjacent curves corresponding to each θ_J in case of $C_\mu \geqq 0.15$ of Fig. 8.

From this Table, it is seen more clearly that θ_{sep} moves parallely corresponding to θ_J.

(2) The case of $\theta_J \geqq 0°$

In this case, as there is not a slot corresponding to the tripwire in $\theta < 0°$, the boundary layer around the cylinder must have separated before the slot and it is found that the boundary layer has really separated at about $-14° \sim -24°$, when $C_\mu = 0$ in Fig. 8.

Though the separation occurs without the influence of the slot, there is a staggering of the separation points. This is thought due to the experimental error.

It is thought due to the same reason that the front-stagnation points are not at $-90°$ (see Fig. 9).

However, it is obvious that the flow is symetric on the upper and lower sides of the cylinder as seen from the curve of $C_\mu = 0$ in Fig. 5c. Therefore, the lift is not generated on the cylinder in this case (see Fig. 4).

If the air is injected into the flow that has separated, the boundary layer is given the momentum in the flow direction even at very small C_μ, is reattached to the surface of the cylinder and the separation point moves largely to downstream

(see Fig. 8).

The rapid increase of C_{pb} in Fig. 10 too corresponds to the large movement of the separation point to downstream.

And the static-pressure distributions of Figs. 5c, 5d, 5e, 5f, too, if the jet of small C_μ is injected, show that the parts of the negative pressure become quickly large and the separation point largely moves to downstream.

Hence, the front-stagnation point fairly largely moves to the negative side of θ (see Fig. 9).

So, the circulation around the cylinder in this case is larger than in case of $C_\mu = 0$ and the lift increases rapidly.

As C_μ is gradually increased, C_L shows the similar tendency as the case of $\theta_J \leqq -20°$, that is, the larger the θ_J is, the larger the C_L is at the same C_μ.

Fig. 7 shows the curves C_P vs. θ of the various θ_J at $C_\mu = 0.231 \pm 0.005$. It is seen from this figure that the larger the θ_J is, the larger the negative pressure is and that the separation point correspondingly moves to downstream.

That is, this corresponds to the fact that the larger the θ_J is the larger the C_L is.

On the other hand, the curves of C_L vs. C_μ at each θ_J are almost mutually parallel.

This can be guessed from Fig. 8 and Table 1 too.

That is, when C_μ is large, the increment of C_L with θ_J is almost independent of C_μ and is determined by only the relative value of θ_J.

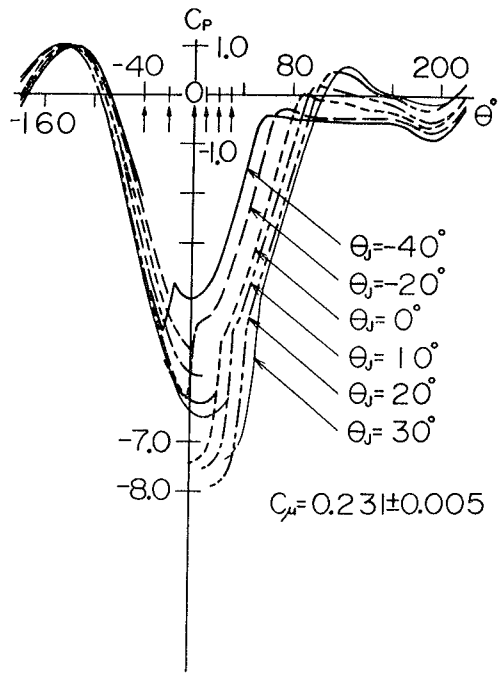

Fig. 7 Static-pressure distributions at various θ_J's when $C_\mu = 0.231$.

Therefore, when C_μ is large, C_L is to be expressed as $C_L = f(C_\mu) + g(\theta_J)$ where $f(C_\mu)$ and $g(\theta_J)$ monotonically increase with C_μ and θ_J respectively. Hence, it is clear that the larger the θ_J is, the better the efficiency of the power required is.

4-2 On the drag coefficient, C_D

It is shown in Fig. 4 that C_D behaves peculiarly at small C_μ depending on each θ_J in the similar way as C_L.

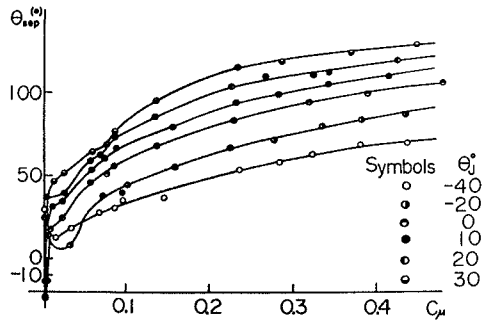

Fig. 8 Angles of separation points.

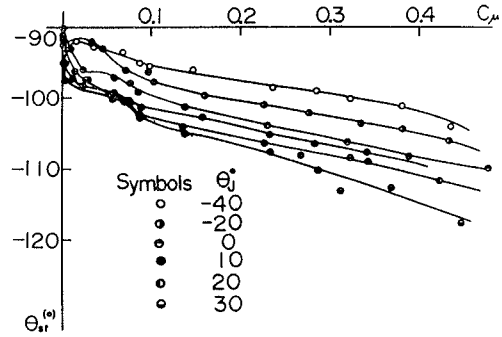

Fig. 9 Angles of front-stagnation points.

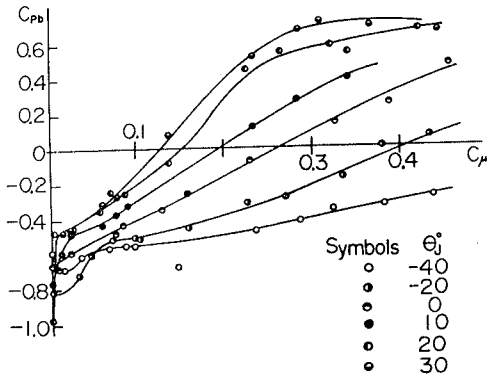

Fig. 10 Base-pressure coefficients.

(1) The case of $\theta_J \leqq -20°$

As C_μ increases starting from 0, C_D tends to increase once and to decrease after reaching the maximum value.

When C_μ is further increased, C_D tends to increase again after passing the local minimum (see Fig. 4).

Generally, the drag based on the pressure difference on the cylinder surface in the direction of the main flow plays the important role in the drag.

In this experiment, the thrust due to the reactionary force of the jet makes a part of the drag.

But, the value of C_D excluding the thrust can be qualitatively discussed, since

Table 1 Increment of θ_{sep} when θ_J varies.

C_μ \ θ_J (°)	−40∼−20	−20 ∼ 0	0 ∼ 10	10 ∼ 20	20 ∼ 30
0.15	12.2	16.4	8.1	9.8	9.8
0.20	13.8	16.5	8.7	10.9	10.8
0.25	14.5	16.8	9.1	10.2	10.2
0.30	15.1	17.3	8.1	9.6	9.6
0.35	15.8	16.2	8.6	8.7	9.2
0.40	16.8	15.9	8.3	8.9	9.1
0.45	18.2	14.9	8.9	7.4	8.3
Average	15.2±3.0	$16.3^{+1.0}_{-1.4}$	$8.5^{+0.6}_{-0.4}$	$9.3^{+1.6}_{-1.9}$	$9.6^{+1.2}_{-1.3}$

the thrust is proportional to C_μ.

Hence, the strength of the drag is determined by the size of the wake and the negative pressure right after the slot.

Therefore, taking account of the influences of the wake and the negative pressure after the slot on the drag, we proceed with our discussion.

In case of $\theta_J = -40°$, as described in 4-1, as C_μ increases starting from 0, the separation point moves to upstream and after reaching the minimum value, it moves to downstream, when C_μ is small (see Fig. 8).

Hence, the larger the C_μ is, the larger the wake becomes and after reaching the maximum value the wake decreases its size.

It is thought from the static-pressure distribution of Fig. 6 that the negative pressure right after the slot is small, hence, the drag due to the wake plays a main role in the total drag, when C_μ is small.

Therefore, it is thought that C_D varies corresponding to the size of the wake.

That is, when C_μ increases starting from 0, C_D reaches the maximum value once and decreases again.

As C_μ is further increased, the separation point moves to farther downstream and the wake becomes smaller (see Fig. 8).

Whereas, it is seen from the static-pressure distribution (see Fig. 5a) that the negative pressure after the slot gradually increases as C_μ increases. And, this negative pressure pulls the cylinder ahead, and decreases the drag acting on the cylinder.

But, it is evident from the figure that after reaching the first local maximum once, the negative pressure decreases, then it increases again and passes the second local maximum and it decreases.

The position of the second local maximum moves to the farther positive side as C_μ becomes larger, which evidently results in more drag.

Therefore, it is thought that when C_μ is large, C_D is nearly constant independent of C_μ from the viewpoint mentioned above.

C_D in case of $\theta_J = -20°$ behaves similarly as in case of $\theta_J = -40°$ when C_μ is small, but when C_μ is large, the static-pressure distribution is qualitatively equal to the static-pressure distribution of $\theta_J = -40°$ parallely moved by 20° to the positive direction of θ (see Fig. 5b).

Hence, the drag becomes larger than that of $\theta_J = -40°$ and C_D increases by degrees as C_μ is increased.

(2) The case of $\theta_J \geqq 0°$

As described in 4-1, when C_μ increases starting from 0, the separation point moves largely to downstream (see Fig. 8) and the wake is small at the small C_μ.

Moreover, the negative pressure right after the slot is not so large either (see Figs. 5c, 5d, 5e, 5f,) and the drag decreases in comparison with the drag at $C_\mu = 0$.

However, as C_μ is increased, the separation point moves to farther downstream (see Fig. 8). And the negative pressure after the slot becomes very large as seen from the static-pressure distributions of Figs. 5c, 5d, 5e and 5f.

Hence, it is thought that the negative pressure after the slot has dominant influence on the drag acting on the cylinder in this case. Therefore, C_D increases rapidly as C_μ increases when C_μ is large.

4-3 Lift-drag ratio, C_L/C_D

Since this is the ratio of the lift to the drag, what was described in 4-1 and 4-2 appears exaggerated (see Fig. 11.)

From the figure, C_L/C_D reaches the maximum value at some point of $C_\mu > 0.4$ when $\theta_J \leqq -20°$, and its value is large too.

It is shown that the larger θ_J is, C_L/C_D reaches the maximum value at the smaller C_μ.

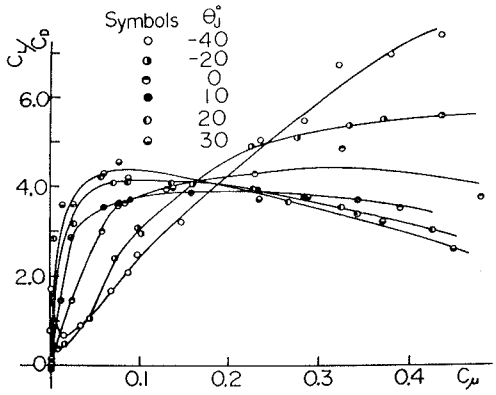

Fig. 11 Lift-drag ratios.

5 Conclusion

It is concluded from the discussion that

1) there exists a large negative pressure right after the slot.
2) when C_μ is small,
   (1) in case of $\theta_J \leqq -20°$, C_L decreases once, reaches the local minimum and increases whereas C_D increases once, gets to the local maximum and decreases as C_μ increases starting from 0.
   (2) in case of $\theta_J \geqq 0°$, C_L increases, first, rapidly and, second, gradually whereas C_D decreases once, gets to the local minimum and increases as C_μ increases starting from 0.
3) when C_μ is large, C_L is qualitatively expressed by the equation, $C_L = f(C_\mu) + g(\theta_J)$ while $\frac{dC_D}{dC_\mu}$ is larger at the larger θ_J.
4) the larger θ_J is, C_L/C_D gets its maximum value at the smaller C_μ and, in fact, the maximum point of C_L/C_D at $\theta_J = -40°$ will be at some point of $C_\mu > 0.4$.

Reference

1) Dunham, J., The Aeron. J. of the Roy. Aeron. Soc., 74, (1970-1), 91.
2) Tanaka and Ueda, Preprint of Japan Soc. Mech. Engrs. (in Japanese), No. 710-15 (1971-8), 65.
3) Yoshino and the other, Reports of The faculty of Engineering of Tottori University, 1-1 (1970-12), 7.
4) Tanner, M., Deutsche Luft-und Raumfahrt Forschungsbericht, 68-08(1968-2).